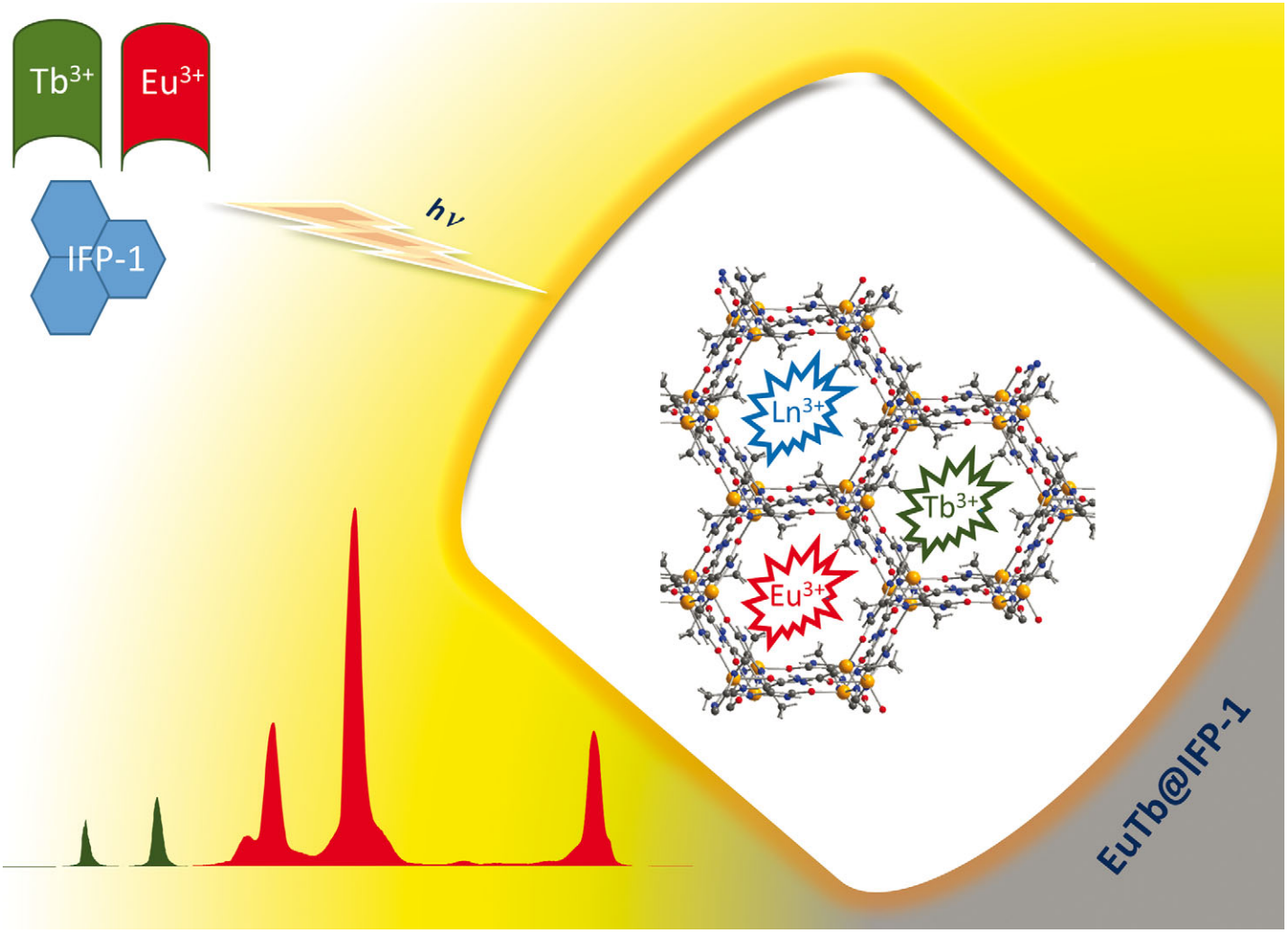

Showcasing research from the research team of Prof. Hans-Jürgen Holdt at Department of Inorganic Chemistry, University of Potsdam, Germany in collaboration with Prof. Klaus Müller-Buschbaum's group at the Institute of Inorganic Chemistry, University of Wurzburg, Germany.

White light emission of IFP-1 by *in situ* co-doping of the MOF pore system with Eu^{3+} and Tb^{3+}

We present the design of a white light emitting microporous MOF with the quality of the three fundamental colors blue, green and red being responsible for the emission of white light from a single source emitter. This is achieved by *in situ* formation and co-doping of the MOF (IFP-1) with lanthanide(III)-ions. The chromaticity point can be shifted and is depending on temperature and the dopant degree of europium and terbium. The microporosity and structure are retained upon intercalation of dopant luminescence centers into the pore system of the MOF.

As featured in:

See Klaus Müller-Buschbaum, Hans-Jürgen Holdt *et al.*, *J. Mater. Chem. C*, 2015, **3**, 4623.

ROYAL SOCIETY OF CHEMISTRY

www.rsc.org/MaterialsC

Registered charity number: 207890

Journal of
Materials Chemistry C

PAPER

View Article Online
View Journal | View Issue

Cite this: J. Mater. Chem. C, 2015, 3, 4623

White light emission of IFP-1 by *in situ* co-doping of the MOF pore system with Eu^{3+} and Tb^{3+}†

Suvendu Sekhar Mondal,[a] Karsten Behrens,[a] Philipp R. Matthes,[b] Fabian Schönfeld,[b] Jörn Nitsch,[b] Andreas Steffen,[b] Philipp-Alexander Primus,[c] Michael U. Kumke,[c] Klaus Müller-Buschbaum*[b] and Hans-Jürgen Holdt*[a]

Co-doping of the MOF $^{3}_{\infty}$[Zn(2-methylimidazolate-4-amide-5-imidate)] (IFP-1 = Imidazolate Framework Potsdam-1) with luminescent Eu^{3+} and Tb^{3+} ions presents an approach to utilize the porosity of the MOF for the intercalation of luminescence centers and for tuning of the chromaticity to the emission of white light of the quality of a three color emitter. Organic based fluorescence processes of the MOF backbone as well as metal based luminescence of the dopants are combined to one homogenous single source emitter while retaining the MOF's porosity. The lanthanide ions Eu^{3+} and Tb^{3+} were doped *in situ* into IFP-1 upon formation of the MOF by intercalation into the micropores of the growing framework without a structure directing effect. Furthermore, the color point is temperature sensitive, so that a cold white light with a higher blue content is observed at 77 K and a warmer white light at room temperature (RT) due to the reduction of the organic emission at higher temperatures. The study further illustrates the dependence of the amount of luminescent ions on porosity and sorption properties of the MOF and proves the intercalation of luminescence centers into the pore system by low-temperature site selective photoluminescence spectroscopy, SEM and EDX. It also covers an investigation of the border of homogenous uptake within the MOF pores and the formation of secondary phases of lanthanide formates on the surface of the MOF. Crossing the border from a homogenous co-doping to a two-phase composite system can be beneficially used to adjust the character and warmth of the white light. This study also describes two-color emitters of the formula Ln@IFP-1a–d (Ln: Eu, Tb) by doping with just one lanthanide Eu^{3+} or Tb^{3+}.

Received 19th December 2014,
Accepted 17th March 2015

DOI: 10.1039/c4tc02919d

www.rsc.org/MaterialsC

1 Introduction

Metal organic frameworks (MOFs) with interesting photophysical properties contribute to the overall variety of functionalities of these inorganic organic hybrid materials.[1–6] MOFs can show effective luminescence by organic chromophore based fluorescence as well as by metal based luminescence processes.[7] This includes different energy transfer mechanisms between linker ligands and metal centers.[8] Similar to today's phosphor converted LED phosphors, co-doping of host lattices with lanthanide ions can be utilized to set a defined amount of luminescence centers in the hybrid material.[9] For a MOF this can in principle be achieved by replacement of the connectivity centers of the framework or by intercalation into cavities of the porous MOF lattice. The choice of the luminescence centers can be used to set the color point of the resulting phosphor. The deliberate choice and mixing of dopants open up a path to tune the color point of the material up to the stage of the emission of white light, as shown for SMOF-1, $In(BTB)_{2/3}(OA)(DEF)_{3/2}$ co-doped with Eu^{3+} (Sandia metal–organic framework-1, BTB: 1,3,5-tris-(4-carboxyphenyl)benzene, OA: oxalic acid, and DEF: *N*,*N*′-diethylformamide).[10] Today, several approaches for color tuning and white light emitting coordination polymers and MOFs have been published.[11] Due to the requirement of a combination of different luminescent species in one homogenous compound to emit white light, each of these white light emitters has been a significant step forward. They exhibit different strategies to achieve white light: co-doping with luminescent metal ions by replacement of the connectivity centers of the framework or the coordination polymer,[11a,b] a controlled setting of metal positions in bimetallic compounds for Ag and Eu,[11c] or a functionalization of pore walls for excitation dependent light emission.[11d]

[a] Institut für Chemie, Anorganische Chemie, Universität Potsdam, Karl-Liebknecht-Straße 26, 14476 Golm, Germany. E-mail: holdt@uni-potsdam.de
[b] Institut für Anorganische Chemie, Universität Würzburg, Am Hubland, 97074 Würzburg, Germany. E-mail: k.mueller-buschbaum@uni-wuerzburg.de
[c] Institut für Chemie, Physikalische Chemie, Universität Potsdam, Karl-Liebknecht-Str. 25, 14476 Golm, Germany

† Electronic supplementary information (ESI) available: Details of IR-spectroscopy, elemental analysis, ICP-OES, powder X-ray diffraction, scanning electron microscopy, energy-dispersive X-ray spectroscopy, thermogravimetric analysis, TG-MS, gas sorption, photoluminescence and decay investigation. See DOI: 10.1039/c4tc02919d

A utilization of the pore system of the MOF for white light emission was achieved by implementing emitting Ir-complexes $[Ir(ppy)_2(bpy)]^+$[11e] as well as luminescent lanthanide ions.[11e] The influence of these procedures on the porosity of the material after filling the pores has not yet been reported. In order to build luminescent functional MOFs synthetic approaches have been developed and such functional MOFs were reviewed recently.[8] The creation of white light has been elaborated by scientists and technicians for a long time with the temperature of the white tone being decisive for the acceptance of new lighting devices and thus the introduction of new technologies.[12] In today's LEDs color mixing by a combination of phosphors (including color converted LED phosphors) is used to set the chromaticity and thus the color point of a light emitter.[13]

We have previously developed a class of metal imidazolate-4-amide-5-imidate based metal organic frameworks called IFP.[14] As is known that Eu^{3+} and Tb^{3+} ions emit red and green light, respectively, it can be expected that zinc metal based IFP-1[14a] co-doped with Eu^{3+} and Tb^{3+} may act as a trichromatic emitter upon retaining the luminescence of all components. Proper mixing can therefore give options for white-light emission. This study reports the solvothermal synthesis of IFP-1 in DMF in the presence of $Eu(NO_3)_3{\cdot}6H_2O$ and $Tb(NO_3)_3{\cdot}5H_2O$, at first for one Ln^{3+} ion at a time [named Ln@IFP-1a–d (Ln = Eu or Tb)] to generate two-color emitters exhibiting the MOF backbone and the Ln^{3+}-emission. Co-doping was then expanded to the simultaneous use of both, Eu^{3+} and Tb^{3+} [named EuTb@IFP-1a–d or a white light emitter], to create three-color white light emitting materials, respectively. We also elaborated the influence of co-doping on the porosity of the MOF by gas adsorption studies (BET) and investigated the luminescence properties, especially tuning of the chromaticity of the emission including the warmth of white light. Finally, the study also describes the border of homogenous doping of the pore system by the formation of lanthanide formates as side phases.

2 Experimental

Materials and synthesis

Ln^{3+} nitrates [$Eu(NO_3)_3{\cdot}5H_2O$ 99.99% trace metals basis and $Tb(NO_3)_3{\cdot}5H_2O$ 99.9% trace metals basis] were used as purchased from Aldrich. DMF was purchased from VWR International. All reagents and solvents were used without further purification.

Synthesis of Ln@IFP-1a–d (Ln = Eu or Tb). $^3_\infty$[Zn(2-methylimidazolate-4-amide-5-imidate)]·$3H_2O$ (IFP-1) was synthesized according to the previously published procedure.[14a] To get lanthanide co-doped materials, the synthetic procedure was modified. The reaction mixture containing $Zn(NO_3)_2{\cdot}4H_2O$ (198 mg, 0.76 mmol) and different equivalents of $Eu(NO_3)_3{\cdot}6H_2O$ or $Tb(NO_3)_3{\cdot}5H_2O$ (from 0.25 to 1.00 equiv.) and 4,5-dicyano-2-methylimidazole (**1**, 100 mg, 0.76 mmol) were dissolved in DMF (6 mL) in a sealed tube. The tube was closed and the mixture was heated up to 110 °C for 72 h and then cooled to room temperature. Crystalline material was formed, which is referred to as Ln@IFP-1a–d in the following report based on the molar ratio of lanthanides and the linker precursor (**1**, Scheme 1 and Table 1).

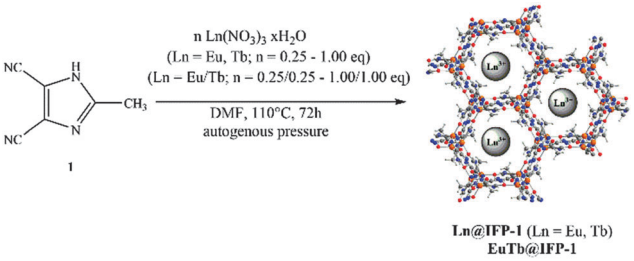

Scheme 1 *In situ* synthesis of single co-doped Eu@IFP-1a–d, Tb@IFP-1a–d and double co-doped EuTb@IFP-1a–d.

Synthesis of EuTb@IFP-1a–d. $Tb(NO_3)_3{\cdot}5H_2O$ (from 0.25/0.25, to 1.00/1.00 equiv.), $Eu(NO_3)_3{\cdot}6H_2O$ (from 0.25/0.25, to 1.00/1.00 equiv.), $Zn(NO_3)_2{\cdot}4H_2O$ (198 mg, 0.76 mmol) and 4,5-dicyano-2-methylimidazole (**1**, 100 mg, 0.76 mmol) were dissolved in DMF (6 mL) in a sealed tube. The reaction mixtures were then treated as described above (Scheme 1 and Table 1). Physical characterization of all materials was done by elemental analysis, inductively coupled plasma atomic emission spectroscopy (ICP-OES) and X-ray powder diffraction (PXRD) (see ESI† for details). To get activated materials, the as-synthesized samples of Ln@IFP-1 were heated to 200 °C at a vacuum of 1×10^{-3} mbar for 48 hours to remove the remaining DMF and water molecules.

3 Results and discussion

Structure determination

The synthesis of luminescent co-doped MOFs is usually based on the statistic replacement of a certain amount of metal ions as connectivity centers by luminescent ions like Ln^{3+} during MOF formation.[9] Statistic replacement is thereby fundamentally dependent on a match between the two different metal ions in parameters like ionic radii, valence and chemical reactivity. For a potential co-doping of IFP-1 with lanthanide ions, these parameters do not match with Zn^{2+}.[15] Accordingly, also options like the formation of heterobimetallic compounds or the utilization of the pore system had to be investigated. On the other hand, the approach of *in situ* ligand synthesis simultaneous to the MOF formation seemed promising to immobilize highly charged ions within the pore system and to thereby avoid a postsynthetic treatment hindered by electrostatic interactions. For the intercalation of lanthanide ions into the MOF pores, the solvothermal reactions of the linker-precursor 4,5-dicyano-2-methylimidazole (**1**) and $Zn(NO_3)_2{\cdot}4H_2O$ were carried out together with different equivalents of nitrates of europium and terbium (Scheme 1 and Table 1).

Ln@IFP-1a–d (Ln = Eu or Tb) and EuTb@IFP-1a–d with amounts of lanthanides up to 14.0 atom% display the PXRD patterns identical to IFP-1 without non-indexed additional reflections (see Fig. 1 for examples and the ESI† details). To get further insights into the real structures of the activated Eu@IFP-1 and Tb@IFP-1 samples, we performed a combination of electron microscopy (SEM) and electron dispersive X-ray

Table 1 Eu- and Tb-single co-doped as well as EuTb-double co-doped IFP-1 samples (all activated) measured by ICP-OES

IFP-1 material co-doped with lanthanides	Equivalents of $Eu(NO_3)_3{\cdot}6H_2O$[a]	$Tb(NO_3)_3{\cdot}5H_2O$[a]	Atom% (product)[b] Eu	Tb	Zn
Eu@IFP-1a	0.25		0.02 ± 0.01		99.98 ± 0.01
Eu@IFP-1b	0.50		0.03 ± 0.02		99.97 ± 0.02
Eu@IFP-1c	0.75		0.48 ± 0.06		99.52 ± 0.06
Eu@IFP-1d	1.00		1.04 ± 0.06		98.96 ± 0.06
Tb@IFP-1a		0.25		0.07 ± 0.02	99.93 ± 0.02
Tb@IFP-1b		0.50		0.11 ± 0.01	99.89 ± 0.01
Tb@IFP-1c		0.75		0.10 ± 0.03	99.90 ± 0.03
Tb@IFP-1d		1.00		0.16 ± 0.01	99.84 ± 0.01
EuTb@IFP-1a	0.25	0.25	0.04 ± 0.02	0.04 ± 0.01	99.93 ± 0.03
EuTb@IFP-1b	0.50	0.50	0.10 ± 0.03	0.11 ± 0.02	99.80 ± 0.05
EuTb@IFP-1c	0.75	0.75	0.91 ± 0.56	0.91 ± 0.54	98.18 ± 1.10
EuTb@IFP-1d	1.00	1.00	7.16 ± 0.24	6.76 ± 0.19	86.07 ± 0.42

[a] Referred to the equivalents of $Zn(NO_3)_2{\cdot}4H_2O$ employed in the synthesis. [b] Atom%, referred to the metal content; determined by ICP-OES.

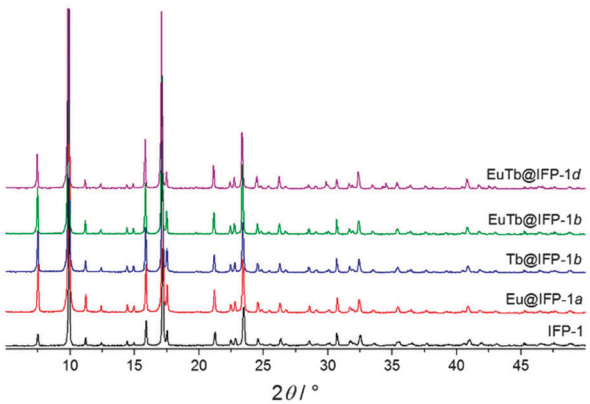

Fig. 1 X-ray powder diffraction patterns of Ln@IFP-1; Cu-K_α radiation (λ = 1.54056 Å).

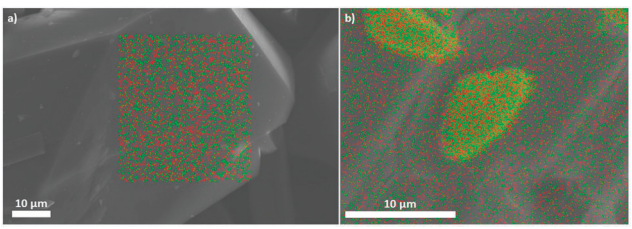

Fig. 2 Eu(red)- and Tb(green)-elemental mapping of (a) of EuTb@IFP-1b and (b) EuTb@IFP-1d.

spectroscopy (EDX). Eu-elemental mapping shows a homogenous distribution of Eu^{3+} for an Eu-content lower than 0.50 atom% (*e.g.* Eu@IFP-1c; Fig. S8 in ESI†).

The Eu- and Tb-elemental mappings of EuTb@IFP-1b also indicate a uniform distribution of lanthanides (Fig. 2a). At higher Eu-contents, the SEM image and the Eu-elemental mapping revealed that additional microcrystals of $Eu(HCOO)_3$ were formed (*e.g.* for 1.04 atom% (Eu@IFP-1d), Fig. S8, ESI†). This is also observed for the referring Eu/Tb co-doped materials. Elemental mapping of EuTb@IFP-1d depicts microcrystals of mixed $EuTb(HCOO)_3$ deposited on the surface of an IFP-1 crystal (Fig. 2b). It can be anticipated that this microscopic difference illustrates the border of homogenous doping of the pore system for EuTb@IFP-1b and inhomogeneous doping for EuTb@IFP-1d, as only the latter shows mixed $EuTb(HCOO)_3$ on the outside of the MOF crystals. The microscopic formation of the secondary phase can be attributed to the decomposition of DMF to formates. It is intriguing that the border of homogenous doping of the MOF cannot be observed by PXRD patterns of Ln@IPF-1, as the method is not suitable to determine very low amounts of secondary phases. Instead combination with other microscopic methods, as done here by SEM and EDX is essential for such modifications of MOFs in order to determine the correct characteristics. Apparently, PXRD can only determine the reflections of $Ln(HCOO)_3$ at much higher concentrations. We therefore also carried out TG-MS measurements to identify $Ln(HCOO)_3$ (see ESI† for details). We selected some of these doped materials for the details of gas sorption and fluorescence studies.

Sorption and porosity

In order to investigate the dependence of doping with lanthanide ions on the microporosity of IFP-1, physisorption experiments were carried out with N_2 at 77 K on non-doped IFP-1 and frameworks homogenously doped with Eu^{3+} (Eu@IFP-1c), Tb^{3+} (Tb@IFP-1d) and Eu^{3+} together with Tb^{3+} (EuTb@IFP-1b), as well as on the MOF material showing the start of microscopic phase separation at a higher dopant degree by formation of $EuTb(HCOO)_3$ on the surface of EuTb@IFP-1d. For further comparison, sorption experiments were also carried out with CO_2 at 195 K on non-doped IFP-1 and Eu@IFP-1c. Specific surface areas were estimated by the use of adsorption isotherms for both N_2 and CO_2 utilizing the Brunauer–Emmet–Teller model (BET).

Adsorption and desorption isotherms indicate microporosity for IFP-1, Eu@IFP-1c and Tb@IFP-1d of the same magnitude, for both N_2 and CO_2 sorption (Fig. 3). The full microporosity of the IFP-1 framework is retained upon doping with lanthanide ions, as long as no phase separation is observed (Table 2).

For dopant degrees lower than 0.50 atom% of Ln^{3+} ions, no blockage of pores is observed besides the equilibration

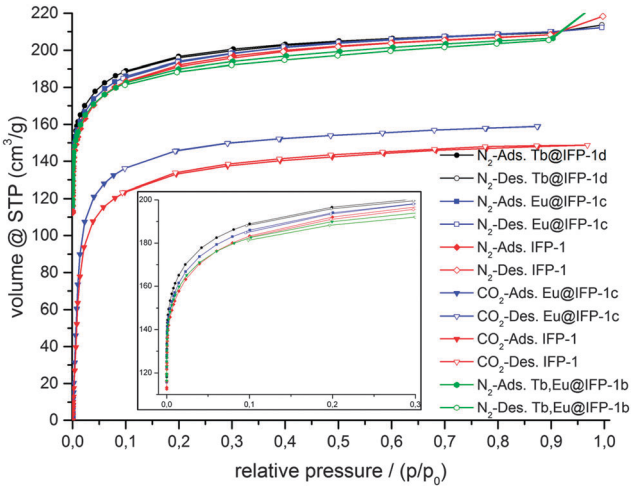

Fig. 3 Adsorption (closed symbols) and desorption isotherms (open symbols) for N_2 sorption at 77 K and CO_2 at 195 K on IFP-1, homogenously doped Eu@IFP-1c, Tb@IFP-1d and EuTb@IFP-1b.

Table 2 Calculated BET-surface areas and total pore volumes of IFP-1, Eu@IFP-1c, Tb@IFP-1d, EuTb@IFP-1b and EuTb@IFP-1d for N_2 and CO_2 adsorption

Sample	Surface area (BET) ($m^2\ g^{-1}$)	Total pore volume ($cm^3\ g^{-1}$)
N_2 on IFP-1	737	0.33
N_2 on Eu@IFP-1c	758	0.33
N_2 on Tb@IFP-1d	745	0.33
N_2 on EuTb@IFP-1b	702	0.31
N_2 on EuTb@IFP-1d	633	0.28
CO_2 on IFP-1	736	0.28
CO_2 on Eu@IFP-1b	768	0.30

hindrance, which should be a sign for homogenous doping that is not only on the outer surface of the MOF, as this would lead to blockage of pores and a loss or stronger reduction of the inner surface. Accordingly, the surface investigations also assume that Eu@IFP-1c, Tb@IFP-1d and EuTb@IFP-1b are homogenously doped porous MOF phosphors. Observed deviations in the surface area between IFP-1 and Ln^{3+}-doped IFP can mostly be addressed to influences of synthesis conditions. Hence, the *in situ* loading of microporous IFP-1 can be successfully carried out without diminishing the porosity of the MOF.

Non-doped IFP-1 shows a total uptake of 208 $cm^3\ g^{-1}$ for N_2 and 148 $cm^3\ g^{-1}$ for CO_2, while doped Eu@IFP-1c and Tb@IFP-1d show total uptakes of 210 $cm^3\ g^{-1}$ for N_2 each, as well as 159 $cm^3\ g^{-1}$ of CO_2 on Eu@IFP-1-c (at relative pressures close to unity). This indicates comparable inner surface areas for non-doped IFP-1 and all homogenously low-doped frameworks investigated (Table 2) despite the different analyte temperatures.

For dopant concentrations higher than 1.00 atom% the gas uptake decreases, as the additional phases of $Ln(HCOO)_3$ are deposited as microcrystals on the outer surface of the homogenous Ln-doped IFP. Even though on a μm scale, they are large enough to block channels of the pore system, as shown for EuTb@IFP-1d. This sealing-off of some part of MOF micropores reduces the inner surface and thus the gas uptake. For an amount of 14 atom% of Eu^{3+} and Tb^{3+} ions, as determined for EuTb@IFP-1d, the observed reduction of the specific surface area is about 14%, equaling 104 $cm^3\ g^{-1}$ and corresponding to a reduced specific surface area of 633 $m^2\ g^{-1}$ for N_2. The option to achieve both, homogenous doping as well as phase separation, further supports the idea that the pore system of IFP-1 can be utilized for doping, but that there are certain limits for the homogenous co-doping of IFP-1 with lanthanide ions.

Because of the chemical and thermal stability of the intrinsic one-dimensional channel structure, the zinc constituted IFP-1 is also formed in the presence of nitrates of Eu^{3+} and Tb^{3+}. It could be anticipated that the lanthanide ions are encapsulated into the channels of IFP-1 and not statistically substituting the connectivity centers, as there is a large mismatch between Zn^{2+} and Ln^{3+} in ionic radii and charge. The presence of the imidate and amide groups of the channel walls and thus the inner surface of IFP-1 enhances the polarization and hydrophilic characteristics of the channels and allows interaction with lanthanide ions. Low-doped Ln@IFP-1 contains only small amounts of Ln^{3+} ions, which introduce an imbalance in the electronic equilibrium of the network that needs to be balanced by a corresponding amount of anions. Based on the analytics described above, we assume an additional intercalation of formate anions. Further electronic exchange for charge equilibration at functional groups is possible inside the channels of the framework.

Photoluminescence

Non-doped IFP-1 exhibits a weak photoluminescence due to a broad, blue emission band ranging from 375 nm to 700 nm at RT with its maximum at λ_{max} = 463 nm (λ_{ex} = 360 nm) (Fig. 4). The excitation band in the range of 300 nm to 425 nm is also broad with its maximum at λ_{max} = 355 nm (λ_{em} = 463 nm) and a shoulder at around $\lambda_{shoulder} \sim$ 430 nm (Fig. S13, ESI†). Doping of the IFP framework by the *in situ* available Eu^{3+} and Tb^{3+} ions during the formation reaction introduces additional luminescence

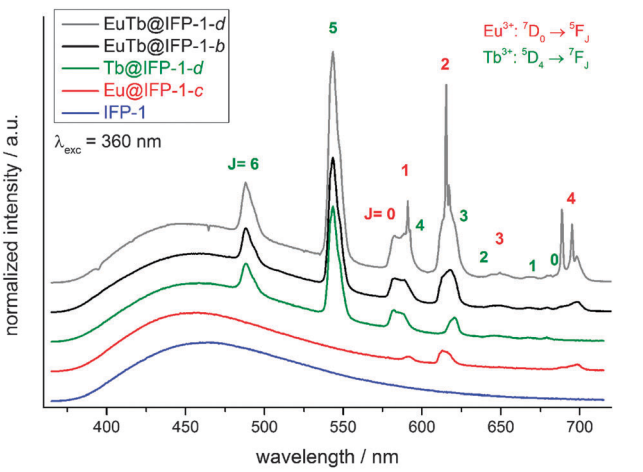

Fig. 4 Emission spectra of IFP-1, the homogenously Ln^{3+}-co-doped Eu@IFP-1c, Tb@IFP-1d and EuTb@IFP-1b, as well as the heterogeneously doped material EuTb@IFP-1d (all as-synthesized) obtained under indirect excitation conditions (λ_{ex} = 360 nm) at RT.

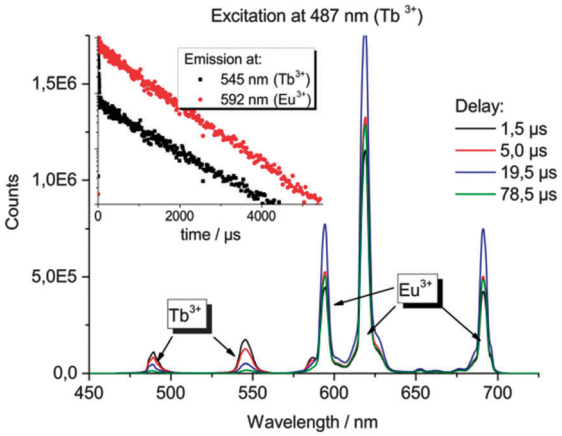

Fig. 5 Emission spectra of EuTb@IFP-1d (as synthesized) with the typical emission bands for Eu^{3+} and Tb^{3+} after direct excitation of Tb^{3+} at λ_{ex} = 487 nm recorded with different delays between excitation and emission measurements. The inset shows the emission decay kinetics for Tb^{3+} and Eu^{3+}.

properties. Besides the framework fluorescence, the lanthanide containing materials, *e.g.* Eu@IFP-1c and Tb@IFP-1d, exhibit additional, characteristic lanthanide emission bands.[16,17] The additional emission bands originate from the corresponding metal-centered 4f–4f transitions of the respective trivalent lanthanide ions in Ln^{3+}-doped IFP-1. The emission can be observed by excitation of the framework ligands, which act as sensitizers for the lanthanide ions establishing an antenna effect[18] (Fig. 4), indicating an energy transfer between the IFP-backbone and the Ln^{3+}-dopants. The direct excitation of the Ln^{3+} 4f–4f transitions is also possible (Fig. 5), but weak compared to the antenna effect. Accordingly, the excitation spectra of doped Eu@IFP-1c and Tb@IFP-1d are very similar to the excitation spectra of non-doped IFP-1 (Fig. S13 at ESI†) because of the low extinction coefficients of the lanthanide ions compared to the framework backbone.

For Tb@IFP-1d, the typical Tb^{3+}-transitions $^5D_4 \rightarrow {}^7F_J$ (J = 6–0) are observed, and for Eu@IFP-1c the Eu^{3+}-transitions $^5D_0 \rightarrow {}^7F_J$ (J = 0–4) are detected. After introduction of the Eu^{3+} or Tb^{3+} ions into the framework, the intensity of the broad emission band of the framework itself does not change significantly. Comparing the intensities of the sensitized Ln^{3+}-emission, the Tb^{3+}-containing compound Tb@IFP-1d shows a more intensive 4f–4f emission than Eu@IFP-1c (Fig. 4). Excitation of co-doped IFP with Eu^{3+} and Tb^{3+} (Fig. 4, EuTb@IFP-1b and EuTb@IFP-1d) leads to the blue framework emission along with the characteristic green and orange-red emissions of Tb^{3+} and Eu^{3+}, respectively.

Framework backbone centered emission and Ln^{3+}-centered emission can also be distinguished by investigations of the decay time of the photoluminescence processes. The decay time of the fluorescence process is on the low nanosecond scale for the broad band emission of the ligand (IFP-1: τ = 0.33(1)–5.74(20) ns, Eu@IFP-1c: τ = 0.13(1)–4.22(14) ns, and Tb@IFP-1d: τ = 0.04(2)–4.82(16) ns), which is much faster than the luminescence decay times found for Eu^{3+} and Tb^{3+} (Eu@IFP-1c: τ = 314(13)–1337(117) µs, and Tb@IFP-1d: τ = 580(33)–1062(60) µs; see also Table S6, ESI†).

In the Eu^{3+}- and Tb^{3+}-co-doped samples, in addition to the antenna effect of the ligand, a metal-to-metal energy transfer from Tb^{3+} to Eu^{3+} was detected for the materials EuTb@IFP-1b and EuTb@IFP-1d. This energy transfer is more effective for higher lanthanide loadings as the efficiency of the energy transfer depends on the average distances between the donor and the acceptor (Fig. 4). Given a random distribution of dopants the distance between Eu^{3+} and Tb^{3+} is inversely proportional to the metal loading. The $Tb^{3+} \rightarrow Eu^{3+}$ metal-to-metal energy transfer is proven by detection of Eu^{3+} emission after selective excitation of Tb^{3+} (λ_{ex} = 478 nm) and the observed luminescence decay kinetics of Tb^{3+} and Eu^{3+}, as shown by site selective PL spectroscopy (Fig. 5). This energy transfer is a great tool to fine-tune the color point and thus the chromaticity of the white light emitting materials. Higher Eu^{3+} emission intensities lead to a warmer white light emission (*vide infra*).

White light emission properties

As stated, the organic part of the framework contributes a broad band emission in the blue spectral range, Tb^{3+} and Eu^{3+} add a green and a red emission component, respectively, to the EuTb-co-doped IFP-1 materials. Altogether this enables the emission of white light by EuTb@IFP-1, as the materials (as shown for EuTb@IFP-1b and EuTb@IFP-1d) exhibit a combination of the framework fluorescence and the luminescence of Tb^{3+} as well as Eu^{3+} (Fig. 4 and 5). The three color emitter EuTb@IFP-1 thereby meets today's standards of color rendering of LED phosphors and exceeds the recent two color emitting MOFs.[10,19] Compared to IFP-1 co-doped with one lanthanide ion, only, like Eu@IFP-1b and d, a significant increase in Eu^{3+}-luminescence intensity is observed contributing to the overall white emission color of the materials EuTb@IFP-1b and EuTb@IFP-1d (Fig. 4 and 5). It is remarkable that EuTb@IFP-1 shows a tunable chromaticity point with varying dopant concentrations (Fig. 6 and Table S5, ESI†).

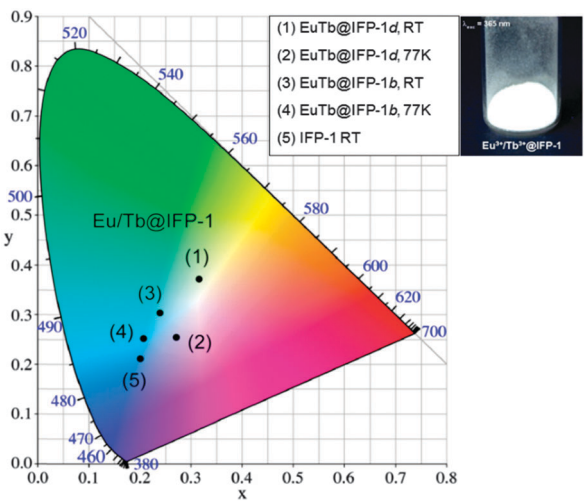

Fig. 6 Chromaticity diagram of as-synthesized EuTb@IFP-1b and EuTb@IFP-1d at room temperature and at 77 K illustrating the dependence of the temperature on the chromaticity point according to CIE and visual impression of the white light emission of as-synthesized EuTb@IFP-1d.

In addition, the temperature can also be used to influence the color point of the materials. One reason is a reduction of the blue ligand emission upon increasing temperature. Consequently, the overall white color temperature of the co-doped IFP is also temperature dependent (Fig. 6). At 77 K, EuTb@IFP-1d emits a cold white light, which turns into a warm white light at RT. Hence the warmth of the white color could also be used for temperature sensing, as recently shown for $Eu_{0.0069}Tb_{0.9931}$–DMBDC (DMBDC: 2,5-dimethoxy-1,4-benzene-dicarboxylate).[11a] The color point is moved further to a warmer color by larger amounts of lanthanide ions. This behavior can be explained by smaller average Tb^{3+}–Eu^{3+} distances and therefore a more effective metal-to-metal energy transfer leading to an increased contribution of the red Eu^{3+} emission to the white light (Fig. 6). It is intriguing that besides the homogenous distribution of the lanthanide ions in the pore system, heterogeneous composites of EuTb@IFP-1 with lanthanide formate crystals on the outer surface can also have beneficial effects on the tuning of the warmth of the white light emission. This further underlines the importance to distinguish between homogenous loading of the pore system of the MOF and a utilization of the outer surface for an understanding of the processes observed.

In order to understand the coordination environment and position of Ln^{3+}-dopants incorporated into the IFP materials during synthesis, high resolution Eu^{3+}-spectra were recorded. At ultra-low temperatures of 4 K, processes contributing to the spectral broadening of electronic transitions (inhomogeneous broadening) are minimized and small differences in the electronic spectra of different chemical species or chemical species in different environments and coordination can be resolved. Site selective Eu^{3+}-spectroscopy using a narrow bandwidth dye laser as an excitation light source offers a unique possibility to probe Eu^{3+} ions and distinguish their different chemical environments. Due to the non-degenerate ground ($^7F_0$) and first excited states ($^5D_0$) of Eu^{3+}, the corresponding electronic transition of a single species of Eu^{3+} ions consists of only one peak, which is not split by the crystal field. The energy of the absorption and emission is dependent on the strength of the crystal field and differs for different Eu^{3+} species (nephelauxetic effect). Subsequently, different chemical species present in one single sample can be probed individually. Moreover, the obtained Stark-splitting patterns of the lower energy transitions $^5D_0 \rightarrow {}^7F_1$–$^7F_6$ contain complementary information on the individual chemical species, *e.g.*, the symmetry and homogeneity of a distinct lattice site. We chose different Eu@IFP-1 samples to elaborate the study on the location and coordination environment of the lanthanide ions.

Homogenously doped Eu@IFP-1b and EuTb@IFP-1b (both as-synthesized) show no sharp, distinct emission lines indicating that the probed Eu^{3+} ions are located in non-homogeneous binding environments (Fig. 7) and not on a distinct crystallographic site, if they replaced the connectivity centers of IFP-1. The broad, unresolved luminescence originates from Eu^{3+} ions distributed over a variety of slightly different chemical environments in the sample, which would be possible inside the pores of the MOF. Based on the luminescence spectra no indication of a separate phase including formate is found, which is in good agreement with the other analytical results (Fig. S8b at ESI† and Fig. 2a, respectively).

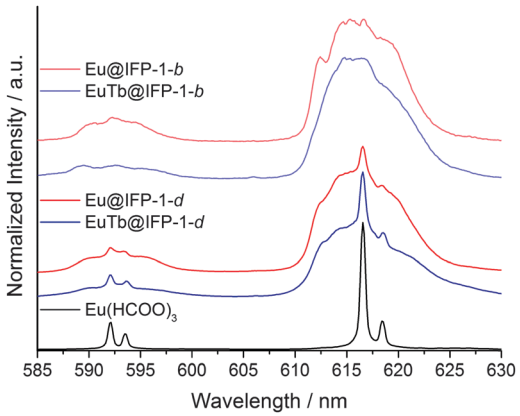

Fig. 7 Emission spectra of $Eu(HCOO)_3$, homogenous/heterogeneous Ln^{3+} co-doped Eu@IPF-1d and EuTb@IPF-1d, as well as homogenous doped Eu@IFP-1b and EuTb@IPF-1b (all as-synthesized) after excitation at λ_{ex} = 579.60 nm, the excitation maximum of $Eu(HCOO)_3$. All spectra are extracted from the total luminescence spectra (as shown in Fig. 6) after a scan over the $^7F_0$–$^5D_0$ transition at T = 4 K.

Site-selective excitation of the $^5D_0 \rightarrow {}^7F_0$ transition of the various doped Eu@IFP-1d and EuTb@IFP-1d materials (both as synthesized) yielded luminescence spectra showing one Eu^{3+} species with a two-fold crystal field splitting of the $^5D_0$–$^7F_1$ and $^5D_0$–$^7F_2$ transitions along with the same broad luminescence without well-resolved Stark-splitting (Fig. 7).

Comparison with a $Eu(HCOO)_3$ reference shows that the sharp, two-fold split luminescence lines can be attributed to the formation of small domains of crystalline $Eu(HCOO)_3$. This again is in very good agreement with the results obtained from SEM and EDX (Fig. S8d, ESI†) and shows that the region of homogenous doping can also be spectroscopically identified by ultra-low temperature PL spectroscopy.

Removal of solvent molecules by heating the Eu@IFP-1d samples to 200 °C in a vacuum of 1 mbar was performed until the sample mass was constant. In the total emission spectra (Fig. 8) two things can be seen: (i) the sharp emission peaks attributed to the formate phase (λ_{ex} = 579.6 nm, *vide supra*) are preserved and (ii) alteration in shape/structure of the broad excitation and emission bands (Fig. 8). Alterations in the spectra always originate from alterations in the crystal field experienced by the Eu^{3+}-dopants. The changes in the broad excitation and emission bands suggest that the Eu^{3+} ions are located inside the channels of IFP-1 from which the solvent escapes, as opposed to an additional (formate) phase and/or the outside surface of the MOF. The changes in the luminescence signature upon removal of solvent molecules from the MOF framework channels, at the same time, strongly support the previously concluded saturation of the coordination spheres of Eu^{3+} by solvent molecules.

Although the emission and excitation bands appear to be overall broadened upon the removal of solvent molecules indicating greater variations in the crystal fields, the increased structure in the emission and excitation spectra is clearly visible. The structure in the spectra can be interpreted as more

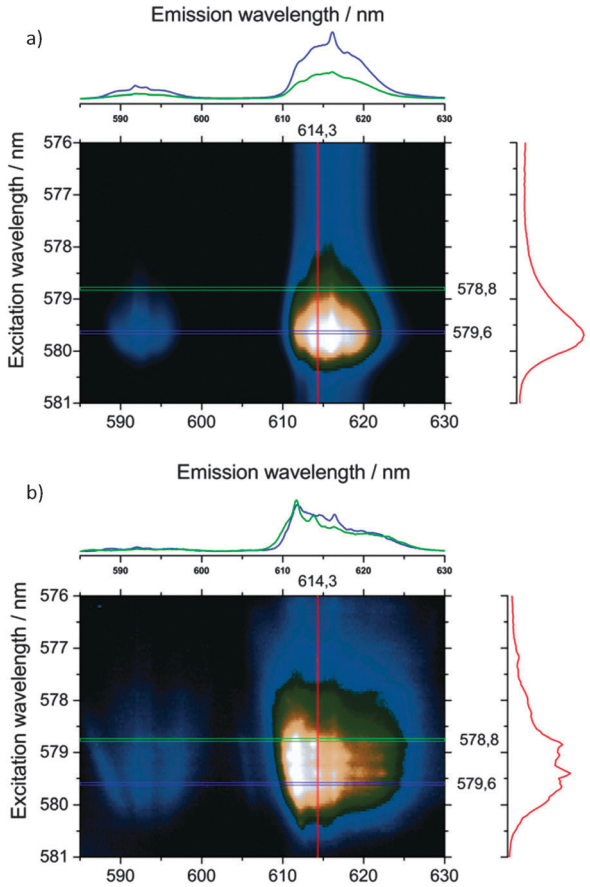

Fig. 8 Total emission spectra (logarithmic intensity/color scale) of Eu@IPF-1d (as-synthesized (top) and activated (bottom)) after excitation of the $^7F_0$–$^5D_0$ transition between λ_{ex} = 576–581 nm at T = 4 K. Note the formate peak at λ_{em} = 616.2 nm and the excitation and emission broadening in the activated sample due to increased general inhomogeneity of the coordination spheres of the dopant ions.

distinct, more crystalline-like crystal sites, where greater numbers of Eu^{3+} ions have very similar coordination spheres and therefore crystal fields.

The colored intensity plots of the total luminescence allow a rough estimation of the number of different lattice sites, meaning groups of Eu^{3+}-dopants experiencing an identical crystal field. About four groups of identical Eu^{3+} ions can be excited in a very narrow bandwidth between 578.8 nm and 579.6 nm for the activated samples, each group showing different emission intensity patterns (Fig. 8b). It seems, due to the relatively rigid structure of the MOF, that there is a limited amount of symmetries that can stabilize the depleted coordination spheres of Eu^{3+}-dopants after removal of solvent molecules, thus explaining the sharpened peaks. This indicates favored positions of the Ln^{3+} ions within the pore system, interacting with the functional groups of the linker. Trapping of Eu^{3+} and Tb^{3+} ions was just recently shown for the MOF $Zn_4O(L)_{1.5}$, L = 6,6′-(2,2-bis((6-carboxy-naphthalen-2-yloxy)methyl)propane-1,3-diyl)bis(oxy)di-2-naphthoate showing a color tuning of the luminescence from green to red at different Eu/Tb ratios.[20a] Capture of Ln^{3+}-ions in MOF pores was also used for the detection of Ln^{3+} by uptake of the ions Eu^{3+} and Tb^{3+} into IFMC, a zinc nitrate MOF with tricarboxylate ligands based on a central tripodal ether group, to give Eu@IFMC-10 and Tb@IFMC-10.[20b]

For EuTb@IFP-1, indirect excitation of europium in the UV spectral range using framework sensitization supports the interpretation that the unstructured, broad emission is caused by Ln^{3+} ions located inside the channels of the MOF material. The antenna effect depends on the close proximity of the metal ion and the sensitizer (MOF channel walls coordinating Ln^{3+}). Thereby, site selective photoluminescence spectroscopy and total emission spectra give vital insights into the nature of the lanthanide uptake in the pores and also corroborate the formation of lanthanide formate side phases from a certain Ln-amount, as the luminescence of both phenomena can be clearly distinguished.

Conclusions

To summarize, the formation of a white light emitting MOF is achieved by simultaneous co-doping of IFP-1 with Tb^{3+} and Eu^{3+} during the *in situ* formation of the ligand and the MOF. This *in situ* co-doping with trivalent Ln^{3+} ions enables luminescent MOFs with almost identical porosity to the non-doped framework. The three emission colors blue, green and red are therefore combined in one emitter. The luminescence of the IFP-1 backbone together with 4f-emission of the lanthanide ions add to a three-color white light emitting MOF that shows the effective white light emission in comparison with the previously known one- and two-color white light emitters. The photoluminescence is supported by ligand-to-metal and metal-to-metal energy transfers, with the color of the white light emission being temperature and Ln^{3+} concentration dependent. A more bluish chromaticity is observed for cooling to 77 K and for low dopant degrees, whereas a warmer white light is emitted at RT for high dopant amounts. This effect can be potentially used for spectroscopic temperature sensing. The lanthanide ions do not replace zinc ions as connectivity centers but are intercalated into the pore system of the IFP-1 MOF during synthesis without a structure directing effect. The uptake is homogenous with no detectable differences in distribution if the final dopant degree is lower than 1.0 atom% referred to the amount of Zn^{2+}. At higher dopant degrees, phase formation of lanthanide formates from decomposition of the solvent DMF starts to occur in addition to the intercalation into the MOF. The lanthanide formates can be characterized as the secondary crystalline phase at the outer surface of the MOF particles and limit the homogenous region of co-doping. Intercalated Ln^{3+} ions and lanthanide formates can be clearly distinguished by means of photoluminescence spectroscopy, SEM/EDX and sorption experiments. Eu- and Tb-formates on the surface can be beneficially used to further tune the chromaticity of the MOF in a composite relationship. The luminescent MOFs Ln@IFP-1 retain their microporosity upon loading with luminescence centers regarding sorption of N_2 at 77 K and CO_2 at 195 K in the homogenous region of co-doping. To the best of our knowledge, EuTb@IFP-1d is the first example of a

white light emitting MOF with proven porosity in combination with luminescence centers inside the pore system and non-substituting connectivity centers of the MOF.

Acknowledgements

The authors thank Dr C. Günter (Universität Potsdam) for help with X-ray powder diffraction measurements, Dr M. Neumann for TG-MS measurements, S. Lubahn (Universität Potsdam) for the ICP-OES measurements and Y. Linde (Universität Potsdam) for the C, H, and N elemental analysis. This work is financially supported by the Priority Program 1362 of the German Research Foundation on "Metal–Organic Frameworks" and the Dr Klaus-Römer foundation.

Notes and references

1 (*a*) J. L. C. Rowsell and O. M. Yaghi, *Microporous Mesoporous Mater.*, 2004, **73**, 3; (*b*) O. M. Yaghi, G. Li and H. Li, *Nature*, 1995, **378**, 703; (*c*) G. J. Férey, C. Mellot-Draznieks, C. Serre and F. Millange, *Acc. Chem. Res.*, 2005, **38**, 217; (*d*) S. L. James, *Chem. Soc. Rev.*, 2003, **32**, 276; (*e*) S. Meek, J. Greathouse and M. Allendorf, *Adv. Mater.*, 2011, **23**, 249; (*f*) M. Li, D. Li, M. O'Keeffe and O. M. Yaghi, *Chem. Rev.*, 2014, **114**, 1343.

2 (*a*) S. Ma and H.-C. Zhou, *Chem. Commun.*, 2010, **46**, 44; (*b*) K. Sumida, D. L. Rogow, J. A. Mason, T. M. McDonald, E. D. Bloch, Z. R. Herm, T.-H. Bae and J. R. Long, *Chem. Rev.*, 2012, **112**, 724; (*c*) M. P. Suh, H. J. Paark, T. K. Prasad and D.-W. Lim, *Chem. Rev.*, 2012, **112**, 782; (*d*) L. J. Murray, M. Dinč and J. R. Long, *Chem. Soc. Rev.*, 2009, **38**, 1294; (*e*) A. U. Czaja, N. Trukhan and U. Müller, *Chem. Soc. Rev.*, 2009, **38**, 1284; (*f*) T. R. Cook, Y.-R. Zheng and P. J. Stang, *Chem. Rev.*, 2013, **113**, 734.

3 (*a*) L. Pan, D. H. Olson, L. R. Ciemnolonski, R. Heddy and J. Li, *Angew. Chem., Int. Ed.*, 2006, **45**, 616; (*b*) J.-R. Li, J. Sculley and H.-C. Zhou, *Chem. Rev.*, 2012, **112**, 869; (*c*) J.-R. Li, R. J. Kuppler and H.-C. Zhou, *Chem. Soc. Rev.*, 2009, **38**, 1477.

4 (*a*) A. M. Shultz, O. K. Farha, J. T. Hupp and S. T. Nguyen, *J. Am. Chem. Soc.*, 2009, **131**, 4204; (*b*) D. J. Lun, G. I. N. Waterhouse and S. G. Telfer, *J. Am. Chem. Soc.*, 2011, **133**, 5806; (*c*) R. E. Morris and X. Bu, *Nat. Chem.*, 2010, **2**, 353.

5 (*a*) X. L. Qi, R. B. Lin, Q. Chen, J. B. Lin, J.-P. Zhang and X.-M. Chen, *Chem. Sci.*, 2011, **2**, 2214; (*b*) Y.-N. Wu, F. Li, W. Zhu, J. Cui, C.-A. Tao, C. Lin, P. M. Hannam and G. Li, *Angew. Chem., Int. Ed.*, 2011, **50**, 12518.

6 (*a*) P. Horcajada, C. Serre, M. Vallet-Regi, M. Sebban, F. Taulelle and G. J. Férey, *Angew. Chem., Int. Ed.*, 2006, **45**, 5974; (*b*) P. Horcajada, C. Serre, G. Maurin, N. A. Ramsahye, F. Balas, M. Vallet-Regi, M. Sebban, F. Taulelle and G. J. Férey, *J. Am. Chem. Soc.*, 2008, **130**, 6774; (*c*) S. Keskin and S. Kizilel, *Ind. Eng. Chem. Res.*, 2011, **50**, 1799.

7 (*a*) Z. Hu, B. J. Deibert and J. Li, *Chem. Soc. Rev.*, 2014, **43**, 5815; (*b*) Q.-Y. Liu, Y.-L. Wang, N. Zhang, Y.-L. Jiang, J.-J. Wie and F. Luo, *Cryst. Growth Des.*, 2011, **11**, 3717; (*c*) K. Liu, H. You, Y. Zheng, G. Jia, L. Zhang, Y. Huang, M. Yang, Y. Song and H. Zhang, *CrystEngComm*, 2009, **11**, 2622; (*d*) H. Zhang, N. Li, C. Tian, T. Liu, F. Du, P. Lin, Z. Li and S. Du, *Cryst. Growth Des.*, 2012, **12**, 670; (*e*) C. J. Höller, M. Mai, C. Feldmann and K. Müller-Buschbaum, *Dalton Trans.*, 2010, **39**, 461.

8 (*a*) M. D. Allendorf, C. A. Bauer, R. K. Bhakta and R. J. T. Houk, *Chem. Soc. Rev.*, 2009, **38**, 1330; (*b*) J. Rocha, L. D. Carlos, F. A. Almeida Paz and D. Ananias, *Chem. Soc. Rev.*, 2011, **40**, 926; (*c*) Y. Cui, Y. Yue, G. Qian and B. Chen, *Chem. Rev.*, 2012, **112**, 1126; (*d*) N. Stock and S. Biswas, *Chem. Rev.*, 2012, **112**, 933; (*e*) J. Heine and K. Müller-Buschbaum, *Chem. Soc. Rev.*, 2013, **42**, 9232; (*f*) Z. Hu, B. J. Deibert and J. Li, *Chem. Soc. Rev.*, 2014, **43**, 5815; (*g*) Y. Cui, B. Chen and G. Qian, *Coord. Chem. Rev.*, 2014, **273**, 76; (*h*) J. Lei, R. Qian, P. Ling, L. Cui and H. Ju, *Trends Anal. Chem.*, 2014, **58**, 71; (*i*) C. Dey, T. Kundu, B. P. Biswal, A. Mallick and R. Banerjee, *Acta Crystallogr., Sect. B: Struct. Sci., Cryst. Eng. Mater.*, 2014, **70**, 3; (*j*) D. Liu, K. Lu, C. Poon and W. Lin, *Inorg. Chem.*, 2014, **53**, 1916; (*k*) Y. F. Chen, Y.-C. Ma and S.-M. Chen, *Cryst. Growth Des.*, 2013, **13**, 4154.

9 (*a*) P. Falcaro and S. Furukawa, *Angew. Chem.*, 2012, **51**, 8431; (*b*) A. Zurawski, M. Mai, D. Baumann, C. Feldmann and K. Müller-Buschbaum, *Chem. Commun.*, 2011, **47**, 496; (*c*) P. R. Matthes, C. J. Höller, M. Mai, J. Heck, S. J. Sedlmaier, S. Schmiechen, C. Feldmann, W. Schnick and K. Müller-Buschbaum, *J. Mater. Chem.*, 2012, **22**, 10179; (*d*) Q. Tang, S. Liu, Y. Liu, D. He, J. Miao, X. Wang, Y. Ji and Z. Zheng, *Inorg. Chem.*, 2014, **53**, 289; (*e*) V. Haquin, M. Etienne, C. Daiguebonne, S. Freslon, G. Calvez, K. Bernot, L. Le Pollès, S. E. Ashbrook, M. R. Mitchell, J.-C. Bünzli, S. V. Eliseeva and O. Guillou, *Eur. J. Inorg. Chem.*, 2013, 3464; (*f*) H. Zhang, X. Shan, L. Zhou, P. Lin, R. Li, E. Ma, X. Guoab and S. Du, *J. Mater. Chem. C*, 2013, **1**, 888; (*g*) J.-C. Rybak, M. Hailmann, P. R. Matthes, A. Zurawski, J. Nitsch, A. Steffen, J. G. Heck, C. Feldmann, S. Götzendörfer, J. Meinhardt, G. Sextl, H. Kohlmann, S. J. Sedlmaier, W. Schnick and K. Müller-Buschbaum, *J. Am. Chem. Soc.*, 2013, **135**, 6896; (*h*) H. Zhang, X. Shan, Z. Ma, L. Zhou, M. Zhang, P. Lin, S. Hu, E. Ma, R. Li and S. Du, *J. Mater. Chem. C*, 2014, **2**, 1367; (*i*) Y. Wang, Y.-Y. Liu and J.-F. Ma, *Chem. – Eur. J.*, 2013, **19**, 14591.

10 D. F. Sava, L. E. S. Rohwer, M. A. Rodriguez and T. M. Nenoff, *J. Am. Chem. Soc.*, 2012, **134**, 3983.

11 (*a*) Q. Tang, S. Liu, Y. Liu, D. He, J. Miao, X. Wang, Y. Ji and Z. Zheng, *Inorg. Chem.*, 2014, **53**, 289; (*b*) A. Ablet, S.-M. Li, W. Cao, X.-J. Zheng, W.-T. Wong and L.-P. Jin, *Chem. – Asian J.*, 2013, **8**, 95; (*c*) Y. Liu, M. Pan, Q.-Y. Yang, L. Fu, K. Li, S.-C. Wei and C.-Y. Su, *Chem. Mater.*, 2012, **24**, 1954; (*d*) F. Luo, M.-S. Wang, M.-B. Luo, G.-M. Sun, Y.-M. Song, P.-X. Lia and G.-C. Guo, *Chem. Commun.*, 2012, **48**, 5989; (*e*) C.-Y. Sun, X.-L. Wang, X. Zhang, C. Qin, P. Li, Z.-M. Su, D.-X. Zhu, G.-G. Shan, K.-Z. Shao, H. Wu and J. Li, *Nat.*

Commun., 2013, **4**, 2717; (*f*) L. V. Meyer, F. Schönfeld and K. Müller-Buschbaum, *Chem. Commun.*, 2014, **50**, 8093.

12 (*a*) S. P. Nakamura, *Proc. SPIE*, 1997, **3002**, 26; (*b*) R. Mueller-Mach, G. O. Mueller, M. R. Krames and T. Trottier, *IEEE J. Sel. Top. Quantum Electron.*, 2002, **8**, 339.

13 (*a*) R. Mueller-Mach, G. O. Mueller, M. R. Krames, H. A. Hoppe, F. Stadler, W. Schnick, T. Juestel and P. Schmidt, *Phys. Status Solidi A*, 2005, **202**, 1727; (*b*) E. F. Schubert, *Light-emitting diodes*, Cambridge University Press, Cambridge, New York, 2006; (*c*) V. Bachmann, C. Ronda, O. Oeckler, W. Schnick and A. Meijerink, *Chem. Mater.*, 2009, **21**, 316; (*d*) T. Nägele, *LED Professional Rev.*, 2008, **10**, 1; (*e*) W. Lv, Y. Jia, Q. Zhao, W. Lü, M. Jiao, B. Shao and H. You, *J. Phys. Chem. C*, 2014, **118**, 4649; (*f*) Y. Zhang, D. Geng, X. Li, J. Fan, K. Li, H. Lian, M. Shang and J. Lin, *J. Phys. Chem. C*, 2014, **118**, 17983; (*g*) G. Li, C. C. Lin, W.-T. Chen, M. S. Molokeev, V. V. Atuchin, C.-Y. Chiang, W. Zhou, C.-W. Wang, W.-H. Li, H. S. Sheu, T.-S. Chan, C. Ma and R.-S. Liu, *Chem. Mater.*, 2014, **26**, 2991.

14 (*a*) F. Debatin, A. Thomas, A. Kelling, N. Hedin, Z. Bacsik, I. Senkovska, S. Kaskel, M. Junginger, H. Müller, U. Schilde, C. Jäger, A. Friedrich and H.-J. Holdt, *Angew. Chem., Int. Ed.*, 2010, **49**, 1258; (*b*) F. Debatin, K. Behrens, J. Weber, I. A. Baburin, A. Thomas, J. Schmidt, I. Senkovska, S. Kaskel, A. Kelling, N. Hedin, Z. Bacsik, S. Leoni, G. Seifert, C. Jäger, C. Günter, U. Schilde, A. Friedrich and H.-J. Holdt, *Chem. – Eur. J.*, 2012, **18**, 11630; (*c*) F. Debatin, J. Möllmer, S. S. Mondal, K. Behrens, A. Möller, R. Staudt, A. Thomas and H.-J. Holdt, *J. Mater. Chem.*, 2012, **22**, 10221; (*d*) S. S. Mondal, A. Bhunia, I. A. Baburin, C. Jäger, A. Kelling, U. Schilde, G. Seifert, C. Janiak and H.-J. Holdt, *Chem. Commun.*, 2013, **49**, 7599; (*e*) S. S. Mondal, S. Dey, I. A. Baburin, A. Kelling, U. Schilde, G. Seifert, C. Janiak and H.-J. Holdt, *CrystEngComm*, 2013, **15**, 9394; (*f*) S. S. Mondal, A. Bhunia, S. Demeshko, A. Kelling, U. Schilde, C. Janiak and H.-J. Holdt, *CrystEngComm*, 2014, **16**, 39; (*g*) S. S. Mondal, A. Bhunia, A. Kelling, U. Schilde, C. Janiak and H.-J. Holdt, *Chem. Commun.*, 2014, **50**, 5441.

15 (*a*) Y.-Q. Sun, J. Zhang, Y.-M. Chen and G.-Y. Yang, *Angew. Chem., Int. Ed.*, 2005, **44**, 5814; (*b*) Y.-Q. Sun, J. Zang and G.-Y. Yang, *Chem. Commun.*, 2006, 4700; (*c*) S.-R. Zheng, S.-L. Cai, Q.-Y. Yang, T.-T. Xia, J. Fan and W.-G. Zhang, *Inorg. Chem. Commun.*, 2011, **14**, 826; (*d*) Z.-H. Zhang, T.-A. Okamura, Y. Hasegawa, H. Kawaguchi, L. Y. Kong, W.-Y. Sun and N. Ueyama, *Inorg. Chem.*, 2005, **44**, 6219; (*e*) S.-M. Li, X. J. Zheng, D.-Q. Yuan, A. Ablet and L.-P. Jin, *Inorg. Chem.*, 2012, **51**, 1201; (*f*) R.-L. Chen, X.-Y. Chen, S.-R. Zheng, J. Fan and W.-G. Zhang, *Cryst. Growth Des.*, 2013, **13**, 4428; (*g*) Q. Tang, S. Liu, Y. Liu, D. He, J. Miao, X. Wang, Y. Ji and Z. Zheng, *Inorg. Chem.*, 2014, **53**, 289.

16 (*a*) J.-C. G. Bünzli and S. V. Eliseeva, in *Basics of Lanthanide Photophysics*, Fluorescence: Lanthanide Luminescence: Photophysical, Analytical and Biological Aspects, ed. O. S. Wolfbeis and M. Hof, Springer Verlag, Berlin, 2011, vol. 7; (*b*) G. H. Dieke, *Spectra and energy levels of rare earth ions in crystals*, Interscience Publishers, New York, 1968.

17 (*a*) J.-C. G. Bünzli and C. Piguet, *Chem. Soc. Rev.*, 2005, **34**, 1048; (*b*) K. Binnemans, *Chem. Rev.*, 2009, **109**, 4283; (*c*) S. V. Eliseeva and J.-C. G. Bünzli, *Chem. Soc. Rev.*, 2010, **39**, 189.

18 (*a*) G. F. de Sá, O. L. Malta, C. de Mello Donegá, A. M. Simas, R. L. Longo, P. A. Santa-Cruz and E. F. da Silva Jr., *Coord. Chem. Rev.*, 2000, **196**, 165; (*b*) F. R. Gonçalves e Silva, O. L. Malta, C. Reinhard, H.-U. Güdel, C. Piguet, J. E. Moser and J.-C. G. Bünzli, *J. Phys. Chem. A*, 2002, **106**, 1670; (*c*) H. Guo, Y. Zhu, S. Qiu, J. A. Lercher and H. Zhang, *Adv. Mater.*, 2010, **22**, 4190.

19 A. Ablet, S.-M. Li, W. Cao, X.-J. Zheng, W.-T. Wong and L.-P. Jin, *Chem. – Asian J.*, 2013, **8**, 95.

20 (*a*) Y.-Q. Lan, H.-L. Jiang, S.-L. Li and Q. Xu, *Adv. Mater.*, 2011, **23**, 5015; (*b*) L. Chen, K. Tan, Y.-Q. Lan, S.-L. Li, K.-Z. Shao and Z.-M. Su, *Chem. Commun.*, 2012, **48**, 5919.